Monthly Notices
of the
ROYAL ASTRONOMICAL SOCIETY

Mon. Not. R. Astron. Soc. **417,** 1672–1683 (2011) doi:10.1111/j.1365-2966.2011.19228.x

Systematics in the gamma-ray burst Hubble diagram

V. F. Cardone,[1⋆] M. Perillo[2,3] and S. Capozziello[3,4]

[1]*INAF – Osservatorio Astronomico di Roma, via Frascati 33, 00040 Monte Porzio Catone (Roma), Italy*
[2]*Dipartimento di Fisica 'E. R. Caianiello', Università di Salerno, Via Ponte Don Melillo, 84081 Fisciano (Sa), Italy*
[3]*INFN – Sez. di Napoli, Compl. Univ. Monte S. Angelo, Ed. G, Via Cinthia, 80126 Napoli, Italy*
[4]*Dipartimento di Scienze Fisiche, Università degli Studi di Napoli 'Federico II', Complesso Universitario di Monte Sant'Angelo, Edificio N, via Cinthia, 80126 Napoli, Italy*

Accepted 2011 June 11. Received 2011 May 5

ABSTRACT

Because of their enormous energy release, which allows us to detect them up to a very high redshift, gamma-ray bursts (GRBs) have recently attracted a lot of interest with regards to probing the Hubble diagram (HD) deep into the matter-dominated era; thus, GRBs complement Type Ia supernovae (SNe Ia). However, with the lack of a local GRB sample, it is not easy to calibrate the scaling relations proposed as an equivalent to the Phillips law to standardize GRBs, because of the need to estimate the GRB luminosity distance in a model-independent way. We consider here three different calibration methods, based on the use of a fiducial ΛCDM model, on cosmographic parameters and on the local regression on SNe Ia. We find that the calibration coefficients and the intrinsic scatter do not significantly depend on the adopted calibration procedure. We then investigate the evolution of these parameters with the redshift. We find no statistically motivated improvement in the likelihood, so the no-evolution assumption is actually a well-founded working hypothesis. Under this assumption, we then consider possible systematics effects on the HDs introduced by the calibration method, the averaging procedure and the homogeneity of the sample, arguing against any significant bias. We nevertheless stress that a larger GRB sample with smaller uncertainties is needed to definitely conclude that the different systematics considered here have indeed a negligible impact on the HDs, thus strengthening the use of GRBs as cosmological tools.

Key words: gamma-ray burst: general – cosmological parameters – distance scale.

1 INTRODUCTION

During the last 15 years, observational evidence has been accumulated from the anisotropy and polarization spectra of the cosmic microwave background radiation (CMBR; de Bernardis et al. 2000; Brown et al. 2009; Komatsu et al. 2011), from the large-scale structure traced by galaxy redshift surveys (Dodelson et al. 2002; Percival et al. 2002; Hawkins et al. 2003; Szalay et al. 2003), from the matter power spectrum (Tegmark et al. 2006; Percival et al. 2007) with the imprints of baryonic acoustic oscillations (Eisenstein et al. 2005; Percival et al. 2010) and from the Hubble diagram (HD) of Type Ia supernovae (SNe Ia; Kowalski et al. 2008; Hicken et al. 2009; Kessler et al. 2009). This evidence definitely supports the cosmological picture of a spatially flat universe with a subcritical matter content ($\Omega_{\rm M} \sim 0.3$), which is undergoing a phase of accelerated expansion. While the observational scenario is now firmly established, the search for the motivating theory is, however, still in its infancy, notwithstanding the many efforts and the plethora of models proposed over the years. Ironically, the problem here is not the lack of a well-established theory, but the presence of too many viable candidates, ranging from the classical cosmological constant (Carroll, Press & Turner 1992; Sahni & Starobinsky 2000) to scalar fields (Peebles & Ratra 2003; Copeland, Sami & Tsujikawa 2006) and higher-order gravity theories (Capozziello & Francaviglia 2008; Nojiri & Odintsov 2008; De Felice & Tsujikawa 2010; Sotiriou & Faraoni 2010). All of these are more or less able to fit the available data.

As so often in science, adding further data is the best strategy to put in order the confusing abundance of theoretical models. In particular, pushing the observed HD to higher redshift would allow us to trace the background evolution of the Universe up to the transition regime from the dark energy driven speed up to the decelerated matter-dominated phase. Moreover, the distance modulus $\mu(z)$ is log-linearly related to the luminosity distance. If the luminosity distance depends on the dark energy equation of state through a double integration, we have to go to large z in order to discriminate among the predictions of different models, when these models predict similar $\mu(z)$ curves at lower redshift. Unfortunately, SNe Ia are not ideally suited to this task, with their present-day

⋆E-mail: winnyenodrac@gmail.com

HD going back to $z_{\rm max} \sim 1.4$ and not extending further than $z \simeq 2$, even for excellent space-based projects such as the Supernova Acceleration Probe (SNAP; Aldering et al. 2004).

Because of their enormous, almost instantaneous energy release, gamma-ray bursts (GRBs) are ideal candidates to go deeper in redshift, the farthest so far being at $z = 8.3$ (Salvaterra et al. 2009). The wide range spanned by their peak energy makes them everything but standard candles. However, the existence of many observationally motivated correlations between redshift-dependent quantities and rest-frame properties (Fenimore & Ramirez-Ruiz 2000; Norris, Marani & Bonnell 2000; Ghirlanda, Ghisellini & Lazzati 2004; Liang & Zhang 2005; Amati et al. 2008) offers the intriguing possibility of turning GRBs into standardizeable candles just as SNe Ia. The use of these scaling relations allows us to infer the GRB distance modulus with an error mainly depending on the correlation intrinsic scatter. Combining the estimates from different correlations, Schaefer (2007, hereafter S07) first derived the GRB HD for 69 objects, while Cardone et al. (2009, hereafter CCD09) used a different calibration method and added a further correlation to update the GRB HD. Many attempts to use GRBs as cosmological tools have been performed since then (see, for example, Firmani et al. 2006; Izzo et al. 2009; Liang et al. 2010; Qi & Lu 2010; and references therein) showing the potential of GRBs as cosmological probes.

It is worth emphasizing that the possibility offered by GRBs to track the HD deep into the matter-dominated epoch does not come easily. There are still two main problems actually to be fully addressed. First, lacking a local GRB sample, all the above correlations have to be calibrated assuming a fiducial cosmological model to estimate the redshift-dependent quantities. As a consequence, we have the so-called circularity problem. This means that we want to use GRB scaling relations to constrain the underlying cosmology, but we need the underlying cosmology to obtain the scaling relations. Different strategies have been proposed to break this circularity. Thus, our first aim here is to investigate whether these are indeed viable solutions and to what extent the residual problem affects the derivation of the HD.

A well-behaved distance indicator should not only be visible to high z and possess scaling relations with as small an intrinsic scatter as possible, but also its physics should be well understood from a theoretical point of view. However, as yet there is no definitive understanding of the GRB scaling relations. So, there is a serious drawback, as we cannot anticipate whether the calibration parameters are redshift-dependent or not. Lacking any theoretical model, in this paper we therefore address this problem in a phenomenological way, adopting two different parameterizations for their evolution with z and allowing for a change in the zero-point only or in both zero-point and slope. It is worth noting that such an analysis has been severely hampered previously by the low statistics in the GRB sample, a problem that we partially overcome here, thanks to the use of the catalogue of 115 GRBs, which has recently been assembled by Xiao & Schaefer (2009, hereafter XS09).

The plan of the paper is as follows. In Section 2, we briefly review the different GRB two-dimensional (2D) correlations known so far. We also present the Bayesian-motivated method that we use in the following to calibrate these, using three different approaches to estimate the GRB luminosity distances. The constraints thus obtained and their dependence on the adopted luminosity distance determination are discussed in Section 3. In Section 4, we address the problem of their dependence on the redshift. The issues related to the derivation of the HD are then discussed in Section 5, where we consider the impact that the averaging procedure and the homogeneity of the sample have on the HD of the luminosity distance estimate method. We give a summary of the main results and we discuss these in Section 6. Finally, some complementary material is presented in the appendix.

2 GAMMA-RAY BURST SCALING RELATIONS

It is instructive to start this analysis considering the general case of two observable quantities (x, y) related by a power-law relation. In a log–log plane, this is

$$\log y = a \log x + b. \tag{1}$$

Calibrating such a relation means determining the slope a, the zero-point b and the scatter $\sigma_{\rm int}$ of the points around the best-fitting relation. In order to be useful for distance determination, one of the two quantities (i.e. x) should refer to a directly observed quantity, while the other must depend on the redshift z. Setting $y = \kappa d_{\rm L}^2(z)$, where κ is a directly measurable redshift-independent quantity and $d_{\rm L}(z)$ is the luminosity distance, we obtain

$$\log y = \log \kappa + 2 \log d_{\rm L}(z) = a \log x + b.$$

Thus, we can then estimate the distance modulus as

$$\mu = 25 + 5 \log d_{\rm L}(z) = 25 + (5/2)\,(a \log x + b - \log \kappa)\,.$$

In order to perform such an estimate, a two-step procedure has to be implemented. First, we have to select a sample of low-redshift ($z \leq 0.01$) objects with known distance and to fit the scaling relation to the (x, y) data, thus estimated to infer the calibration parameters $(a, b, \sigma_{\rm int})$. Secondly, we have to assume that such calibration parameters do not change with the redshift. So, a measurement of (x, κ, z) and the use of the above scaling relation, with $(a, b, \sigma_{\rm int})$ the same at all z, are sufficient to infer the distance modulus.

Both these steps are daunting tasks for GRBs because of the lack of low-redshift objects to be used in the calibration procedure. In order to overcome this problem, different strategies can be implemented. However, their impact on the final derivation of the GRB HD have not been investigated in detail; this is our aim here.

2.1 Two-dimensional empirical correlations

Their high luminosity means that it is possible to detected GRBs at very large z. This means that GRBs are promising candidates to trace the HD in the matter-dominated era. In the last few years, much effort has been devoted to looking for reliable and narrow empirical correlations. Here, we consider only 2D correlations because these can be investigated with a larger number of GRBs. These involve a wide range of GRB properties, related to both the energy spectrum and the light curve, which are then correlated with the isotropic luminosity L or the emitted collimation corrected energy E_γ. Neither L nor E_γ are directly measurable quantities as they depend on the luminosity distance $d_{\rm L}(z)$. Indeed, we have

$$L = 4\pi d_{\rm L}^2(z) P_{\rm bolo}, \tag{2}$$

$$E_\gamma = 4\pi d_{\rm L}^2(z) S_{\rm bolo} F_{\rm beam} (1+z)^{-1}. \tag{3}$$

Here, $P_{\rm bolo}$ and $S_{\rm bolo}$ are the bolometric peak flux and fluence, respectively, and $F_{\rm beam} = 1 - \cos(\theta_{\rm jet})$ is the beaming factor, where $\theta_{\rm jet}$ is the rest-frame time of the achromatic break in the afterglow light curve. Note that the bolometric quantities are related to the observed quantities as (S07)

$$P_{\rm bolo} = P \frac{\int_{1/(1+z)}^{10^4/(1+z)} E\,\Phi(E)\,{\rm d}E}{\int_{E_{\rm min}}^{E_{\rm max}} E\,\Phi(E)\,{\rm d}E}, \tag{4}$$

$$S_{\rm bolo} = S\frac{\int_{1/(1+z)}^{10^4/(1+z)} E\Phi(E)\,{\rm d}E}{\int_{E_{\rm min}}^{E_{\rm max}} E\Phi(E)\,{\rm d}E}. \quad (5)$$

Here, P and S are the observed peak energy and fluence, respectively, and $(E_{\rm min}, E_{\rm max})$ are the detection thresholds of the observing instrument. We model the energy spectrum $\Phi(E)$ as a smoothly broken power law (Band et al. 1993):

$$\Phi(E) = \begin{cases} AE^{\alpha}\exp\left[-\dfrac{(2+\alpha)E}{E_{\rm peak}}\right] & \dfrac{E}{E_{\rm peak}} \leq \dfrac{\alpha-\beta}{2+\alpha} \\ BE^{\beta} & \text{otherwise} \end{cases}. \quad (6)$$

The GRB 2D correlations are obtained by setting $y = L$ or $y = E_\gamma$ in equation (1), while different choices are available for x. In particular, we consider the following possibilities: (i) $x = E_{\rm peak}(1+z)/300$ where $E_{\rm peak}$ is the peak energy (in keV) of the fluence spectrum; (ii) $x = \tau_{\rm lag}(1+z)^{-1}/0.1$ where $\tau_{\rm lag}$ (in s) is the time offset between the arrival of the low- and high-energy photons; (iii) $x = \tau_{\rm RT}(1+z)^{-1}/0.1$ where $\tau_{\rm RT}$ (in s) is the shortest time over which the light curve rises by half the peak flux of the burst; (iv) $x = V(1+z)/0.02$ where V is the variability that quantifies the smoothness of the light curve itself. Note that all these quantities are expressed in the GRB rest frame, which motivates the redshift term, while the further scaling constant is introduced to minimize the correlation among errors.

The combination of x and y gives rise to the different correlations we consider:[1] E_γ–$E_{\rm peak}$ (Ghirlanda et al. 2004; Ghirlanda, Ghisellini & Firmani 2006); L–$E_{\rm peak}$ (Schaefer 2003; Yonekotu et al. 2004); L–$\tau_{\rm lag}$ (Norris et al. 2000); L–$\tau_{\rm RT}$ (S07); L–V (Fenimore & Ramirez-Ruiz 2000; Reichart et al. 2001; S07). These five correlations have been used by S07 to derive a combined HD for 69 GRBs. This was later updated by CCD09, who also considered a sixth correlation between the break time $T_{\rm a}$ and the luminosity at break time $L_X(T_{\rm a})$ of the X-ray afterglow (Dainotti, Cardone & Capozziello 2008; Dainotti et al. 2010, 2011).

Recently, a larger catalogue of GRBs has been compiled by XS09. For each object, this gives the values of the different quantities (if available) needed to check the five correlations listed above. We use this sample here as input for our analysis and we refer the interested reader to XS09 for details about the construction of the catalogue and the determination of the observable quantities.

2.2 Bayesian fitting procedure

Equation (1) is a linear relation, which can be fitted to a given data set (x_i, y_i) in order to determine the two calibration parameters (a, b). Moreover, although there is still no theoretical model that explains any of the empirical 2D correlations in terms of GRB physics, we nevertheless expect that the wide range of GRB properties makes the objects scatter around this (unknown) idealized model. As a consequence, the above linear relations will be affected by an intrinsic scatter $\sigma_{\rm int}$, which has to be determined together with the calibration coefficients (a, b). To this aim, in the following we resort to a Bayesian-motivated technique (D'Agostini 2005). Thus, we maximize the likelihood function $\mathcal{L}(a, b, \sigma_{\rm int}) = \exp[-L(a, b, \sigma_{\rm int})]$ with

$$L(a, b, \sigma_{\rm int}) = \frac{1}{2}\sum \ln\left(\sigma_{\rm int}^2 + \sigma_{Y_i}^2 + a^2\sigma_{X_i}^2\right) + \frac{1}{2}\sum \frac{(Y_i - aX_i - b)^2}{\sigma_{\rm int}^2 + \sigma_{Y_i}^2 + a^2\sigma_{X_i}^2} \quad (7)$$

with $(X_i, Y_i) = (\log x_i, \log y_i)$, and the sum is over the $\mathcal{N}$ objects in the sample. Note that, actually, this maximization is performed in the two-parameter space $(a, \sigma_{\rm int})$ as b can be estimated analytically as

$$b = \left[\sum \frac{Y_i - aX_i}{\sigma_{\rm int}^2 + \sigma_{Y_i}^2 + a^2\sigma_{X_i}^2}\right]\left[\sum \frac{1}{\sigma_{\rm int}^2 + \sigma_{Y_i}^2 + a^2\sigma_{X_i}^2}\right]^{-1}. \quad (8)$$

Thus, we no longer consider this as a fit parameter.

It is worth noting that the Bayesian approach allows us to discover what is the most likely set of parameters within a given theory, but it does not tell us whether this model fits the data well or not. An easy way to quantitatively estimate the goodness of the fit obtained is to consider the median and root mean square of the best-fitting residuals, defined as $\delta = Y_{\rm obs} - Y_{\rm fit}$, which we also compute for the different 2D correlations we consider.

The Bayesian approach used here also allows us to quantify the uncertainties on the fit parameters. To this aim, for a given parameter p_i, we first compute the marginalized likelihood $\mathcal{L}_i(p_i)$ by integrating over the other parameter. The median value for the parameter p_i is then found by solving

$$\int_{p_{i,\rm min}}^{p_{i,\rm med}} \mathcal{L}_i(p_i)\,{\rm d}p_i = \frac{1}{2}\int_{p_{i,\rm min}}^{p_{i,\rm max}} \mathcal{L}_i(p_i)\,{\rm d}p_i. \quad (9)$$

The 68 per cent (95 per cent) confidence range $(p_{i,\rm l}, p_{i,\rm h})$ is then found by solving

$$\int_{p_{i,\rm l}}^{p_{i,\rm med}} \mathcal{L}_i(p_i)\,{\rm d}p_i = \frac{1-\varepsilon}{2}\int_{p_{i,\rm min}}^{p_{i,\rm max}} \mathcal{L}_i(p_i)\,{\rm d}p_i, \quad (10)$$

$$\int_{p_{i,\rm med}}^{p_{i,\rm h}} \mathcal{L}_i(p_i)\,{\rm d}p_i = \frac{1-\varepsilon}{2}\int_{p_{i,\rm min}}^{p_{i,\rm max}} \mathcal{L}_i(p_i)\,{\rm d}p_i, \quad (11)$$

with $\varepsilon = 0.68\,(0.95)$ for the 68 per cent (95 per cent) range. Actually, in order to sample the parameter space, we use a Markov chain Monte Carlo (MCMC) method, running two parallel chains and using the Gelman & Rubin (1992) test to check convergence. The confidence ranges are then obtained by considering the histograms of the parameters from the merged chain after burn in cut and thinning.

2.3 Gamma-ray burst luminosity distances

A preliminary step in the analysis of all the 2D correlations mentioned above is the determination of the luminosity L or the collimated energy E_γ, entering as a Y variable in the Y–X scaling laws. As shown by equations (2) and (3), first we have to determine the GRB luminosity distance over a redshift range where the linear Hubble law no longer holds. As such, we should estimate the luminosity distance as

$$d_{\rm L}(z) = \frac{c(1+z)}{H_0}\int_0^z \frac{{\rm d}z'}{E(z')}. \quad (12)$$

Here, $H_0 = 100\,h\,{\rm km\,s^{-1}\,Mpc^{-1}}$ is the present-day Hubble constant and $E(z) = H(z)/H_0$ is the dimensionless Hubble parameter, which depends on the adopted cosmological model, thus leading to the well-known circularity problem (i.e. we would like to use GRBs to

[1] Hereafter, we refer to the correlation obtained by setting $x = X$ and $y = Y$ in equation (1) as the Y–X correlation or the scaling law.

probe the cosmological model, but we need the cosmological model itself to obtain the GRB HD).

Different strategies have been developed to tackle this problem. The simplest is to assume a fiducial cosmological model and to determine its parameters by fitting (e.g. the SNe Ia HD). Because it agrees with a wide set of data, the ΛCDM model is usually adopted as the fiducial cosmological model. Thus, we set

$$E^2(z) = \Omega_{\rm M}(1+z)^3 + \Omega_\Lambda, \tag{13}$$

where $\Omega_\Lambda = 1 - \Omega_{\rm M}$ because of the spatial flatness assumption. In order to determine the parameters $(\Omega_{\rm M}, h)$, we maximize the likelihood function $\mathcal{L}(\Omega_{\rm M}, h) \propto \exp(-\chi^2/2)$ with

$$\chi^2(\Omega_{\rm M}, h) = \sum_{i=1}^{\mathcal{N}_{\rm SNe\,Ia}} \left[\frac{\mu_i^{\rm obs} - \mu^{\rm th}(z_i, \Omega_{\rm M}, h)}{\sigma_{\mu_i}}\right]^2 + \left(\frac{\omega_{\rm M}^{\rm obs} - \omega_{\rm M}^{\rm th}}{\sigma_{\omega_{\rm M}}}\right)^2 + \left(\frac{h^{\rm obs} - h}{\sigma_h}\right)^2. \tag{14}$$

As input data, we use the Union2 SNe Ia sample (Amanullah et al. 2010) to obtain $(\mu_i^{\rm obs}, \sigma_{\mu_i})$ for $\mathcal{N}_{\rm SNe\,Ia} = 557$ objects over the redshift range (0.015, 1.4) and to set $(\omega_{\rm M}^{\rm obs}, \sigma_{\omega_{\rm M}}) = (0.1356, 0.0034)$ for the matter physical density $\omega_{\rm M} = \Omega_{\rm M}h^2$ and $(h, \sigma_h) = (0.742, 0.036)$ for the Hubble constant, in agreement with the results of the *Wilkinson Microwave Anisotropy Probe 7* (*WMAP7*; Komatsu et al. 2011) and Supernova H_0 for the Equation of State (SHOES; Riess et al. 2009) teams, respectively. The best-fitting values are $(\Omega_{\rm M}, h) = (0.261, 0.722)$, while the median value and confidence ranges are

$$\Omega_{\rm M} = 0.259^{+0.019\ +0.032}_{-0.016\ -0.028}, \qquad h = 0.723^{+0.025\ +0.046}_{-0.025\ -0.045}.$$

Although the ΛCDM model fits the data remarkably well, it is nevertheless worth noting that a different cosmological model would give different values for $d_{\rm L}(z)$ and hence different values for (L, E_γ). Thus, this affects the estimate of the calibration parameters $(a, \sigma_{\rm int})$. Although CCD09 have shown that this effect is quite small for a large range of phenomenological dark energy models,[2] it is nevertheless worth being conservative and looking for model-independent approaches. A first step towards this aim is to resort to cosmography (Weinberg 1972; Visser 2004); that is, to expand the scale-factor $a(t)$ to the fifth-order and then to consider the luminosity distance as a function of the cosmographic parameters. Indeed, such a kinematic approach only relies on the validity of the assumption of the Robertson–Walker metric, while no assumption on either the cosmological model or the theory of gravity is needed because the Friedmann equations are never used. We use the expansion of $d_{\rm L}(z)$ to the fifth-order in z as found in Capozziello, Cardone & Salzano (2008) and we determine the Hubble constant h, the deceleration q_0, the jerk j_0, the snap s_0 and the lerk l_0 parameters by fitting the Union2 SNe Ia data, with the prior on h coming from the SHOES team as mentioned above. Note that, in this case, the likelihood function is defined as before, but the pseudo-χ^2 is now given by equation (14) without the term depending on $\omega_{\rm M}$ because now $\Omega_{\rm M}$ is no longer a parameter. Using a similar MCMC algorithm (but now running three parallel chains), we find as best-fitting values:

$$(h, q_0, j_0, s_0, l_0) = (0.741, -0.56, 0.66, -0.41, 3.59).$$

The median values and confidence ranges are

$$h = 0.741^{+0.036\ +0.071}_{-0.035\ -0.072}, \qquad q_0 = -0.45^{+0.05\ +0.10}_{-0.05\ -0.14},$$

$$j_0 = 0.00^{+0.13\ +0.79}_{-0.12\ -0.35}, \qquad s_0 = 0.29^{+0.74\ +1.57}_{-0.20\ -1.08},$$

$$l_0 = -0.07^{+4.77\ +12.27}_{-4.71\ -10.86},$$

in good agreement with previous results in the literature (Bouhmadi-López, Capozziello & Cardone 2010; Vitagliano et al. 2010; Xu & Wang 2010) using different data sets.

As a further step towards a fully model-independent estimate of the GRB luminosity distances, we can use SNe Ia as distance indicators, based on the naïve observation that a GRB at redshift z must have the same distance modulus as a SN Ia having the same redshift. Thus, interpolating the SNe Ia HD gives the value of $\mu(z)$ for a subset of the GRB sample with $z \leq 1.4$, which can then be used to calibrate the 2D correlations (Kodama et al. 2008; Liang et al. 2008; Wei & Zhang 2009). Assuming that this calibration is redshift-independent, we can then build up the HD at higher redshifts using the calibrated correlations for the remaining GRBs in the sample. CCD09 have used a similar approach based on the local regression technique (Cleveland 1979; Cleveland & Devlin 1988; Loader 1999). This combines much of the simplicity of linear least-squares regression with the flexibility of non-linear regression. The basic idea relies on fitting simple models to localized subsets of the data to build up a function that describes the deterministic part of the variation in the data, point by point. Actually, we are not required to specify a global function of any form to fit a model to the data, so there is no ambiguity in the choice of the interpolating function. Indeed, at each point, a low-degree polynomial is fit to a subset of the data containing only those points that are nearest to the point whose response is being estimated. The polynomial is fit using weighted least-squares with a weight function that quickly decreases with the distance from the point where the model has to be recovered. We apply local regression to estimate the distance modulus $\mu(z)$ from the Union2 SNe Ia sample, following the steps schematically sketched in CCD09. We refer the reader to CCD09 for further details and a demonstration of the reliability of the inferred luminosity distances.

3 CALIBRATION PARAMETERS

While the X quantities are directly observed for each GRB, the determination of Y (either the luminosity L or the collimated energy E_γ) is needed for the object's luminosity distance. The three methods described above allow us to obtain three different values for Y. Thus, it is worth investigating whether this has any significant impact on the calibration parameters $(a, b, \sigma_{\rm int})$ for the correlations of interest. Hereafter, we refer to the three samples with the Y quantities estimated using the luminosity distance from the fiducial ΛCDM cosmological model, the cosmographic parameters and the local regression method as the *F*, *C* and *LR* samples, respectively.

As a preliminary caveat, it is worth noting that the error on Y comes from two different contributions. First, there is the uncertainty obtained by propagating these on the observed quantities (i.e. the flux P and the Band parameters for L and the fluence S, the jet angle $\theta_{\rm jet}$ and again the Band parameters for E_γ), which we assume to be uncorrelated. Secondly, there is the uncertainty on

[2] CCD09 adopted the CPL (Chevallier & Polarski 2001; Linder 2003) parametrization of the dark energy equation of state, $w = w_0 + w_a z/(1+z)$, and explored the dependence of $(a, \sigma_{\rm int})$ on (w_0, w_a) for different values of $\Omega_{\rm M}$. While clear trends of $(a, \sigma_{\rm int})$ with $(\Omega_{\rm m}, w_0, w_a)$ were obtained, the relative change is negligibly small. It is worth noting, however, that the calibration parameters might change more if the adopted cosmological model is radically different from the ΛCDM model (see, for example, Diaferio, Ostorero & Cardone 2011, for an illuminating example).

Table 1. Constraints on the calibration parameters $(a, b, \sigma_{\rm int})$ for the 2D correlations considered in the text. The columns are as follows: (1) correlation ID; (2) number of GRBs used; (3) reduced χ^2; (4) best-fitting parameters; (5)–(7) median values and 68 per cent confidence ranges for $(a, b, \sigma_{\rm int})$, respectively. For each correlation, there are three rows, referring to the results obtained using the *F*, *C* and *LR* distances.

ID	$\mathcal{N}$	χ^2/d.o.f.	$(a, b, \sigma_{\rm int})_{\rm bf}$	a	b	$\sigma_{\rm int}$
L–$E_{\rm peak}$	39	1.05	(1.05, 49.75, 0.46)	$0.99^{+0.21\,+0.41}_{-0.22\,-0.43}$	$49.61^{+0.64\,+1.14}_{-0.21\,-0.97}$	$0.46^{+0.08\,+0.16}_{-0.05\,-0.11}$
L–$E_{\rm peak}$	39	1.04	(1.06, 49.66, 0.47)	$1.02^{+0.21\,+0.44}_{-0.20\,-0.43}$	$49.53^{+0.57\,+1.15}_{-0.10\,-0.71}$	$0.47^{+0.07\,+0.15}_{-0.05\,-0.10}$
L–$E_{\rm peak}$	39	1.08	(0.95, 50.00, 0.43)	$0.84^{+0.23\,+0.47}_{-0.23\,-0.44}$	$50.02^{+0.68\,+1.24}_{-0.21\,-0.72}$	$0.45^{+0.05\,+0.17}_{-0.07\,-0.12}$
L–$\tau_{\rm lag}$	27	1.07	(−0.70, 51.60, 0.47)	$-0.65^{+0.17\,+0.36}_{-0.16\,-0.31}$	$51.60^{+0.12\,+0.25}_{-0.05\,-0.17}$	$0.48^{+0.06\,+0.19}_{-0.06\,-0.11}$
L–$\tau_{\rm lag}$	27	1.09	(−0.68, 51.57, 0.47)	$-0.64^{+0.14\,+0.28}_{-0.15\,-0.33}$	$51.60^{+0.07\,+0.17}_{-0.08\,-0.21}$	$0.49^{+0.08\,+0.20}_{-0.07\,-0.13}$
L–$\tau_{\rm lag}$	27	1.09	(−0.67, 51.67, 0.43)	$-0.62^{+0.15\,+0.27}_{-0.14\,-0.33}$	$51.70^{+0.10\,+0.18}_{-0.07\,-0.18}$	$0.44^{+0.07\,+0.16}_{-0.06\,-0.12}$
L–$\tau_{\rm RT}$	31	1.16	(−1.09, 51.81, 0.45)	$-1.02^{+0.24\,+0.46}_{-0.19\,-0.47}$	$51.82^{+0.05\,+0.12}_{-0.04\,-0.10}$	$0.46^{+0.08\,+0.20}_{-0.06\,-0.11}$
L–$\tau_{\rm RT}$	31	1.20	(−1.03, 51.78, 0.46)	$-0.92^{+0.25\,+0.47}_{-0.24\,-0.49}$	$51.83^{+0.04\,+0.10}_{-0.07\,-0.15}$	$0.48^{+0.08\,+0.18}_{-0.07\,-0.13}$
L–$\tau_{\rm RT}$	31	1.10	(−1.07, 51.88, 0.40)	$-0.97^{+0.22\,+0.45}_{-0.22\,-0.47}$	$51.88^{+0.07\,+0.14}_{-0.02\,-0.10}$	$0.41^{+0.07\,+0.15}_{-0.06\,-0.11}$
L–V	37	1.10	(0.34, 52.60, 0.61)	$0.33^{+0.18\,+0.43}_{-0.20\,-0.52}$	$52.53^{+0.25\,+0.56}_{-0.16\,-0.47}$	$0.62^{+0.10\,+0.20}_{-0.07\,-0.14}$
L–V	37	1.09	(0.40, 52.65, 0.61)	$0.37^{+0.21\,+0.49}_{-0.25\,-0.50}$	$52.66^{+0.16\,+0.54}_{-0.30\,-0.69}$	$0.63^{+0.09\,+0.23}_{-0.08\,-0.14}$
L–V	37	1.10	(0.37, 52.73, 0.56)	$0.33^{+0.19\,+0.41}_{-0.22\,-0.52}$	$52.64^{+0.24\,+0.52}_{-0.22\,-0.61}$	$0.57^{+0.09\,+0.13}_{-0.07\,-0.13}$
E_γ–$E_{\rm peak}$	14	1.17	(1.77, 46.71, 0.17)	$1.71^{+0.22\,+0.44}_{-0.24\,-0.65}$	$47.01^{+0.23\,+1.01}_{-0.58\,-1.09}$	$0.20^{+0.07\,+0.19}_{-0.06\,-0.10}$
E_γ–$E_{\rm peak}$	14	1.21	(1.71, 46.80, 0.18)	$1.62^{+0.24\,+0.51}_{-0.29\,-0.64}$	$47.28^{+0.27\,+1.10}_{-0.71\,-1.35}$	$0.21^{+0.07\,+0.16}_{-0.06\,-0.11}$
E_γ–$E_{\rm peak}$	14	1.16	(1.72, 46.81, 0.17)	$1.66^{+0.26\,+0.55}_{-0.28\,-0.57}$	$47.16^{+0.38\,+0.95}_{-0.66\,-1.31}$	$0.20^{+0.07\,+0.18}_{-0.07\,-0.14}$
$E_{\rm iso}$–$E_{\rm peak}$	40	0.79	(1.58, 49.16, 0.52)	$1.54^{+0.27\,+0.55}_{-0.26\,-0.50}$	$49.26^{+0.45\,+1.03}_{-0.45\,-1.04}$	$0.51^{+0.09\,+0.21}_{-0.07\,-0.13}$
$E_{\rm iso}$–$E_{\rm peak}$	40	0.81	(1.24, 49.57, 0.52)	$1.00^{+0.37\,+0.75}_{-0.33\,-0.62}$	$50.16^{+0.99\,+1.69}_{-0.30\,-1.27}$	$0.52^{+0.11\,+0.24}_{-0.08\,-0.16}$
$E_{\rm iso}$–$E_{\rm peak}$	40	0.79	(1.22, 50.03, 0.51)	$1.04^{+0.35\,+0.73}_{-0.38\,-0.70}$	$50.09^{+0.97\,+1.77}_{-0.27\,-1.26}$	$0.52^{+0.12\,+0.27}_{-0.08\,-0.15}$

$d_{\rm L}(z)$, which we estimate from the MCMC chain for the *F* and *C* cases, while it is output from the method for the *LR* case. It is worth noting that, given the large SNe Ia sample used in the fit of ΛCDM and cosmographic parameters and in the local regression technique, the error on the luminosity distance is actually quite small and always smaller than the one from the measurement uncertainties. It is this latter term that we should minimize in order to obtain better-determined *L* and/or E_γ values and thus to put stronger constraints on the slope, zero-point and intrinsic scatter.

In order to constrain the calibration parameters $(a, b, \sigma_{\rm int})$, we can use the Bayesian procedure described above with the three GRB samples as input to the likelihood analysis. However, the *F*, *C* and *LR* samples cannot contain the same number of objects as the GRB luminosity distance (and hence the *Y* quantities) can be estimated only for $z_{\rm min} \leq z \leq z_{\rm max}$ with $(z_{\rm min}, z_{\rm max})$ depending on the adopted method. If we rely on the fiducial ΛCDM model, we can predict $d_{\rm L}(z)$ at every z so that $(z_{\rm min}, z_{\rm max}) = (0, \infty)$. The only caveat is that we are implicitly assuming that a model fitted over the range (0.015, 1.4) probed by the Union2 SNe Ia sample can be extrapolated to the full evolutionary history of the Universe. The *C* sample is based on the use of the cosmographic parameters fitted to the data, after checking that the fifth-order expansion of $d_{\rm L}(z)$ is reliable over the Union2 SNe Ia redshift range. However, the larger z is, the higher the order we have to include in the $d_{\rm L}(z)$ Taylor series to obtain accurate results. Thus, we must set $(z_{\rm min}, z_{\rm max}) = (0, 1.4)$ in order not to bias the determination of the *Y* quantities because of an inaccurate distance approximation. Finally, the local regression method can only be applied to estimate $d_{\rm L}(z)$ over the redshift range probed by the data used for the interpolation. Thus, we obtain the constraint $(z_{\rm min}, z_{\rm max}) = (0.015, 1.4)$. In order to homogenize the three samples, we therefore fit the 2D correlations using only *F*, *C* and *LR* GRBs with $z \leq 1.4$. Thus, we can meaningfully compare the results for the three distance estimate methods.

Table 1 summarizes the constraints on the calibration parameters for the three different samples. Note that we have also included the $E_{\rm iso}$–$E_{\rm peak}$ correlation (Amati, Frontera & Guidorzi 2009) with $E_{\rm iso} = E_\gamma/F_{\rm beam}$. Although this refers to the same quantities used in the E_γ–$E_{\rm peak}$ correlation, it is based on a larger number of GRBs (given that we do not need a measurement of the jet opening angle $\theta_{\rm jet}$). As a general result, we find that the fit is always quite good, with reduced χ^2 values close to 1 in all cases, independent of the 2D correlation considered and the distance estimate method adopted. As such, the results from the different samples are statistically equivalent and can be safely compared.

Although the 68 and 95 per cent confidence ranges for the calibration parameters $(a, b, \sigma_{\rm int})$ for a given correlation overlap quite well for the *F*, *C* and *LR* samples, the best-fitting coefficients and the median values clearly show that the calibration based on the fiducial ΛCDM model leads to steeper scaling laws in most cases. In contrast, shallower slopes are obtained using the *C* or *LR* samples with the *L*–*V* relation as a unique exception.[3] Although the differences in the slopes are not statistically meaningful because of the large uncertainties, it is nevertheless worth investigating whether such an effect can be ascribed to the distance determination. To this end, for a given GRB and *Y*–*X* correlation, let us define the

[3] Actually, the *L*–*V* relation is the shallowest and has the largest intrinsic scatter among the six 2D correlations investigated in this paper. Thus, the different trend of the slope with the sample could also be a statistical artefact.

following quantities:

$$\Delta_X Y = (a_1 X + b_1) - (a_2 X + b_2) = (a_1 - a_2)X + (b_1 - b_2),$$

$$\Delta_{d_L} Y = 2 \log [d_{L1}(z)/d_{L2}(z)].$$

While $\Delta_X Y$ gives the difference in the Y values predicted using the correlations with coefficients (a_1, b_1) and (a_2, b_2), $\Delta_{d_L} Y$ quantifies the effect of estimating the model-dependent quantity Y using two different luminosity distances. Should the change in the slope be the outcome of compensating the offset because of different luminosity distance assumptions, we should obtain $\Delta_X Y \simeq \Delta_{d_L} Y$. Actually, this is not the case. Considering, for example, the L–$E_{\rm peak}$ correlation, a weighted average gives

$$\langle \Delta_X Y \rangle = 0.19 \neq \langle \Delta_{d_L} Y \rangle = 0.09$$

using the F and C samples and

$$\langle \Delta_X Y \rangle = -0.25 \neq \langle \Delta_{d_L} Y \rangle = -0.02$$

for the F versus LR samples. We therefore find that the change in the slope is not induced by the different luminosity distances adopted. Actually, the use of different samples also has an impact on the intrinsic scatter determination with the LR sample, leading to smaller best-fitting and median $\sigma_{\rm int}$ values for all six correlations considered. Because a and $\sigma_{\rm int}$ correlate, the change in the slope is not only a result of the change in the luminosity distances, but also of the intrinsic scatter. Discriminating between these two effects and quantifying their respective contributions is not possible, so we cannot draw any definitive conclusion about the impact of the calibration method on the slope of the 2D scaling relations.

4 EVOLUTION WITH REDSHIFT

As more and more data are added to the available GRB data set, the observational evidence for the six 2D correlations we are considering becomes more and more reliable. However, a clear theoretical motivation is still lacking in many cases. As a consequence, it is also unclear whether the calibration parameters $(a, b, \sigma_{\rm int})$ evolve with the redshift or not. To investigate this issue, we consider two different possibilities for the evolution with z. First, we consider the possibility that the slope is constant, but the zero-point is evolving. In particular, we assume

$$y = B(1+z)^{\alpha} x^A \longrightarrow Y = \alpha \log(1+z) + aX + b, \qquad (15)$$

with $(X, Y) = (\log x, \log y)$ and $(a, b) = (A, \log b)$. Table 2 summarizes the constraints on the $(a, b, \alpha, \sigma_{\rm int})$ parameters obtained by fitting equation (15) to the $z \leq 1.4$ GRBs with distances estimated from the fiducial ΛCDM model. The constraints from the fit to the C and LR samples are consistent within the 68 per cent confidence ranges. Thus, we report these in the appendix for completeness, and we no longer discuss these here.

A comparison with the constraints in Table 1 highlights some interesting lessons. First, we note that both the best-fitting and median values of the slope parameter a are significantly shallower than in the no-evolution case. However, the 68 per cent confidence ranges typically overlap quite well. Thus, from a statistical point of view, such a result should not be overrated. Actually, the addition of one more parameter introduces a degeneracy between a and α so we can make the best-fitting Y–X relation shallower, compensating for the difference in the term aX with the contribution from $\alpha(1+z)$. Indeed, α is typically quite large; the only exception is the E_γ–$E_{\rm peak}$ correlation, which is also the only one with the same best-fitting slope for the fits with and without the evolution term. Quite surprisingly, the no-evolution result (i.e. $\alpha = 0$) is consistent with the 68 per cent confidence range only for the E_γ–$E_{\rm peak}$ correlation. Thus, this argues in favour of an evolution of the calibration parameters with z. However, the reduced χ^2 values are never smaller than those obtained for the fits with no evolution. Moreover, the intrinsic scatter is almost the same for both cases, so allowing for a redshift evolution does not lead to statistically preferred results. As such, we consider a more conservative option to assume that the GRB scaling relations explored here do not evolve with z.

Actually, such a conclusion is model-dependent. As an alternative parametrization, we therefore allow for an evolution of the slope and not only the zero-point of the 2D correlations. We fit the data using

$$Y = (a_0 + a_1 z)X + (b_0 + b_1 z) \qquad (16)$$

(i.e. we are Taylor expanding to first-order the unknown dependence of the slope and zero-point on the redshift). Note that, actually, we should limit the redshift range to very low z to have a meaningful expansion, but we extrapolate this linear relation to any z as a first-order guess, avoiding the addition of further unknown fitting parameters. Moreover, as we expect (a_1, b_1) to be quite small, we skip to logarithmic units for these quantities in order to be more sensitive to the tiny values. Table 3 summarizes the results for the fit to the F sample, while qualitatively similar conclusions can be drawn from comparing these to the C and LR samples, as can be inferred from Table A2 in the appendix.

As a general result, we find that the best-fitting parameters and the median values of the evolutionary coefficients $(\log a_1, \log b_1)$ are typically quite small, indicating that the dependence of both the slope and the zero-point on the redshift is quite weak, if present at

Table 2. Constraints on the calibration parameters $(a, b, \alpha, \sigma_{\rm int})$ for the 2D correlations considered in the text and fitted to the F sample. The columns are as follows: (1) correlation ID; (2) reduced χ^2; (3) best-fitting parameters; (4)–(7) median values and 68 per cent confidence ranges for the fit parameters. The number of GRBs used is the same as in Table 1.

ID	χ^2/d.o.f.	$(a, b, \alpha, \sigma_{\rm int})_{\rm bf}$	a	b	α	$\sigma_{\rm int}$
L–$E_{\rm peak}$	1.08	(0.89, 50.77, 0.67, 0.41)	$0.82^{+0.20}_{-0.19}$	$50.75^{+0.59}_{-0.65}$	$0.68^{+0.18}_{-0.30}$	$0.44^{+0.06}_{-0.06}$
L–$\tau_{\rm lag}$	1.10	(−0.58, 50.38, 0.88, 0.39)	$-0.57^{+0.12}_{-0.14}$	$50.39^{+0.66}_{-0.58}$	$0.87^{+0.30}_{-0.33}$	$0.41^{+0.07}_{-0.06}$
L–$\tau_{\rm RT}$	1.16	(−0.79, 51.22, 0.65, 0.44)	$-0.64^{+0.21}_{-0.25}$	$50.97^{+0.70}_{-0.75}$	$0.76^{+0.36}_{-0.33}$	$0.47^{+0.07}_{-0.06}$
L–V	1.23	(−0.10, 50.27, 1.07, 0.54)	$-0.05^{+0.26}_{-0.37}$	$50.29^{+0.91}_{-0.96}$	$1.04^{+0.52}_{-0.50}$	$0.57^{+0.11}_{-0.08}$
E_γ–$E_{\rm peak}$	1.37	(1.57, 50.64, 0.00, 0.14)	$1.48^{+0.23}_{-0.26}$	$50.42^{+0.51}_{-0.57}$	$0.13^{+0.31}_{-0.28}$	$0.20^{+0.07}_{-0.06}$
$E_{\rm iso}$–$E_{\rm peak}$	0.81	(1.39, 51.58, 0.58, 0.48)	$1.29^{+0.28}_{-0.28}$	$51.57^{+0.84}_{-0.81}$	$0.58^{+0.44}_{-0.45}$	$0.50^{+0.10}_{-0.08}$

Table 3. Constraints on the calibration parameters (a_0, $\log a_1$, b_0, $\log b_1$, $\sigma_{\rm int}$) for the 2D correlations considered in the text and fitted to the F sample. The columns are as follows: (1) correlation ID; (2) reduced χ^2; (3) best-fitting parameters; (4)–(8) median values and 68 per cent confidence ranges for the fit parameters. The number of GRBs used is the same as in Table 1.

ID	χ^2/d.o.f.	$(a_0, \log a_1, b_0, \log b_1, \sigma_{\rm int})_{\rm bf}$	a_0	$\log a_1$	b_0	$\log b_1$	$\sigma_{\rm int}$
L–$E_{\rm peak}$	1.12	(0.89, −2.69, 51.49, −0.21, 0.41)	$0.89^{+0.22}_{-0.25}$	$-3.05^{+2.13}_{-3.63}$	$51.87^{+0.19}_{-0.46}$	$-0.78^{+0.64}_{-3.06}$	$0.44^{+0.03}_{-0.05}$
L–$\tau_{\rm lag}$	1.13	(−0.60, −4.43, 51.31, −0.07, 0.40)	$-0.64^{+0.16}_{-0.19}$	$-2.78^{+1.61}_{-2.85}$	$51.61^{+0.49}_{-0.45}$	$-0.28^{+0.27}_{-2.83}$	$0.43^{+0.08}_{-0.06}$
L–$\tau_{\rm RT}$	1.17	(−1.56, −0.08, 52.38, −0.70, 0.44)	$-0.95^{+0.33}_{-0.46}$	$-1.81^{+1.59}_{-3.90}$	$52.42^{+0.19}_{-0.53}$	$-1.81^{+1.60}_{-3.91}$	$0.47^{+0.07}_{-0.06}$
L–V	1.36	(−0.15, −2.16, 51.40, 0.03, 0.52)	$-0.10^{+0.41}_{-0.44}$	$-1.79^{+1.49}_{-4.81}$	$51.85^{+0.39}_{-0.53}$	$-0.77^{+0.76}_{-2.86}$	$0.58^{+0.10}_{-0.08}$
E_γ–$E_{\rm peak}$	1.70	(0.79, 0.04, 50.37, −0.56, 0.10)	$1.40^{+0.23}_{-0.47}$	$-1.70^{+1.63}_{-2.67}$	$50.61^{+0.08}_{-0.15}$	$-2.86^{+1.91}_{-3.84}$	$0.17^{+0.08}_{-0.06}$
$E_{\rm iso}$–$E_{\rm peak}$	0.79	(0.94, −0.23, 52.00, −0.15, 0.49)	$1.27^{+0.33}_{-0.50}$	$-1.78^{+1.61}_{-2.54}$	$52.56^{+0.16}_{-0.34}$	$-1.73^{+1.42}_{-2.41}$	$0.50^{+0.10}_{-0.08}$

all.[4] However, the slope and zero-point at $z = 0$ are consistent within the 68 per cent confidence range with the corresponding quantities in the no-evolution case. Moreover, the reduced χ^2 values are typically larger than in the no-evolution case, so this latter assumption is statistically preferred.

5 GAMMA-RAY BURST HUBBLE DIAGRAM

Once the calibration parameters for a given Y–X correlation have been obtained, it is then possible to estimate the distance modulus of a given GRB from the measured value of X. Indeed, for a given Y, the luminosity distance is

$$d_{\rm L}^2(z) = y/\kappa$$

with $\kappa = 4\pi P_{\rm bolo}$, $\kappa = 4\pi S_{\rm bolo} F_{\rm beam}/(1+z)$ and $\kappa = 4\pi S_{\rm bolo}/(1+z)$ for $Y = L$, $Y = E_\gamma$ and $E_{\rm iso}$, respectively. Using the definition of distance modulus and estimating Y from X through the Y–X correlation, we then obtain

$$\begin{aligned}\mu(z) &= 25 + 5\log d_{\rm L}(z)\\ &= 25 + (5/2)\log(y/\kappa)\\ &= 25 + (5/2)(aX + b - \log\kappa),\end{aligned} \tag{17}$$

where (a, b) are the best-fitting coefficients for the given Y–X correlation. Note that here we refer only to the fits with no redshift evolution of the calibration parameters, because the analysis in the previous section has not shown any clear evidence for a redshift dependence of (a, b). Although such a result is model-dependent (as we have considered only two possible evolution parametrizations) and is actually limited only to the redshift range $0.015 \leq z \leq 1.4$, we are nevertheless confident that the possible bias induced by the no-evolution assumption is smaller than the present-day measurement uncertainties. However, such an issue is worth reconsidering when a larger and more precise sample becomes available.

Equation (17) allows us to compute the central value of the distance modulus, relying on the measured values of the GRB observables (i.e. those entering the quantity κ) and the best-fitting coefficients (a, b) of the used correlation. However, both κ and (a, b) are known within their own uncertainties, which have to be propagated to obtain the error on $\mu(z)$. Moreover, each correlation is affected by an intrinsic scatter, which has to be taken into account in the total error budget. To this end, we adopt the procedure schematically sketched as follows.

(i) Fix $(a, \sigma_{\rm int})$ to the ith value of the Markov chain and estimate b from equation (8).

(ii) Set the quantities needed to compute X and hence κ randomly sampling from Gaussian distributions centred on the measured observed values and with variance equal to the measurement error.

(iii) Compute μ from equation (17) for all 2000 X values generated above and estimate the mean of the distribution.

(iv) Repeat steps (ii) and (iii) for all points along the chain and estimate the statistical error on μ by symmetrizing the 68 per cent confidence range of the distribution thus obtained.

(v) Add in quadrature the statistical error and the intrinsic scatter $\sigma_{\rm int}$ of the correlation to finally obtain the total uncertainty on the distance modulus μ.

Equation (17) and the above procedure allow us to build up the HD for all GRBs with measured values of the quantities entering a given Y–X correlation. It is then possible both to reduce the uncertainties and (partially) to remove the hidden systematic errors by averaging over the different correlations available for a given GRB. Following S07, we finally estimate the distance modulus for the ith GRB in the sample at redshift z_i as

$$\mu(z_i) = \left[\sum_j \mu_j(z_i)/\sigma^2_{\mu_j}\right]\left[\sum_j 1/\sigma^2_{\mu_j}\right]^{-1}. \tag{18}$$

The uncertainty is given by

$$\sigma_\mu = \left[\sum_j 1/\sigma^2_{\mu_j}\right]^{-1}, \tag{19}$$

where the sum runs over the 2D empirical laws, which can be used for the GRB considered.

As summarized in Table 1 and discussed in Section 3, the best-fitting calibration parameters depend on the method used to set the GRB luminosity distances. Although such a dependence is not statistically meaningful, with the confidence ranges for the different cases being well overlapped, it is nevertheless worth investigating whether they have an impact on the derived HD. Moreover, averaging over more than one correlation implicitly assumes that all of them are physically motivated (i.e. they are the outcome of an unknown underlying theoretical mechanism) and not the artefact of some selection effect that is not well understood. It is therefore also important to check what the effect should be of a possible misleading assumption. Both these issues are discussed in the following.

[4] Note that, as we are using logarithmic units, the no-evolution case cannot be exactly achieved corresponding to $\log a_1$ and $\log b_1$ going to $-\infty$. However, needless to say, obtaining, for example, $\log a_1 \simeq -2$ is the same as stating that there is no evolution at all. Note also that we have implicitly assumed that both a_1 and b_1 are positive. We have, however, checked that the qualitative conclusions are not affected by this assumption.

5.1 Impact of the calibration method

Fig. 1 shows the GRB HDs obtained by averaging over the six 2D correlations, and using the three different calibration methods. As a guide for the eye, the red solid line is the expected $\mu(z)$ curve for the fiducial ΛCDM model. Note that we have excluded GRBs that deviate from this line more than $1\sigma_\Lambda$, where σ_Λ is the rms of $\mu_{\rm fid} - \mu(z)$ for the full sample. Such a criterion is actually quite loose, excluding only two objects out of 114. Thus, we are confident that no bias is induced by this cut.

As a general remark, we find that, notwithstanding the calibration method adopted, the GRB HDs reasonably follow the ΛCDM curve, although with a non-negligible scatter. Quite surprisingly, the scatter is significantly larger in the range $0.4 \leq z \leq 1.4$ because of a set of GRBs with $\mu(z)$ lying systematically above the ΛCDM prediction. We should argue for a failure of the theoretical model, but there is actually a set of points that are hard to reconcile with any reasonable dark energy model. While this could be removed from the sample by an iterative selection procedure, we prefer to err on the conservative side in order to introduce any bias induced by an a priori choice of a dark energy model. It is nevertheless likely that these GRBs are outliers of one or more of the 2D scaling laws used to infer their distance modulus. Looking in detail at their $\mu(z)$ estimates, we find that the estimates obtained from the different correlations entering the averaging procedure are quite different; however, this is not for the GRBs deviating less from the red line. Such a naïve observation makes us argue in favour of a problem with the measurement of the quantities entering the correlations of interest or of a deviation from one of the best-fitting scaling relations. To investigate in detail this issue on a case-by-case basis, it would be necessary to retrieve the original data for each GRB, which is outside our aim in this paper.

In order to compare the HDs from the three different calibration methods, we consider the values of $\Delta\mu = \mu_{\rm fid}(z) - \mu(z)$ with $\mu_{\rm fid}(z)$, the theoretically predicted distance modulus for the fiducial ΛCDM model. We find

$$\langle\Delta\mu\rangle = -0.15, \qquad (\Delta\mu)_{\rm med} = 0.07, \qquad (\Delta\mu)_{\rm rms} = 1.15,$$

$$\langle\Delta\mu\rangle = -0.10, \qquad (\Delta\mu)_{\rm med} = 0.16, \qquad (\Delta\mu)_{\rm rms} = 1.15,$$

$$\langle\Delta\mu\rangle = -0.24, \qquad (\Delta\mu)_{\rm med} = -0.01, \qquad (\Delta\mu)_{\rm rms} = 1.21,$$

for the *F*, *C* and *LR* samples, respectively. We could naïvely be surprised that the *F* sample (whose calibration is based on the same fiducial ΛCDM model used as a reference here) does not give systematically smaller deviations. Actually, the calibration is made using only GRBs with $z \leq 1.4$, but the full sample is dominated by higher z objects. Thus, the mean and median of $\Delta\mu$ are not biased by the choice of the reference model. As a consequence, we find that the rms $\Delta\mu$ is roughly the same for the three samples, although the mean values suggest that the calibration based on the linear regression leads to μ values that are preferentially larger than expected. From a different point of view, higher μ values at high z argue in favour of a model where the transition from deceleration to acceleration takes place at a larger z, which can be achieved (for a dark energy model with constant equation of state) by pushing w_0 to values smaller than -1 (i.e. going to the phantom regime) or decreasing the matter content. However, such a naïve argument should be reconsidered, taking into account the uncertainties on the single GRB distance modulus estimates.

Actually, from the point of view of the impact of calibration methods, we are not interested in minimizing the mean or median values of $\Delta\mu$, but rather on comparing the $\Delta\mu$ distributions among them. Should these distributions be equal, then we could conclude that the HDs based on different calibration methods are consistent with each other. The different mean and median values seem to suggest that this is not the case. However, these distributions are quite asymmetric, and wide enough to allow for a considerable overlap among them. Moreover, for each single GRB, the values of $\Delta\mu$ are consistent with each other within the uncertainties. We can therefore conclude that the HDs obtained using different calibration methods are consistent with each other within the uncertainties.

Nevertheless, we warn the reader that such a result is partially a result of the large error bars. Should these be reduced, the consistency among the three different HDs could also be lost. To this end, however, we should first reduce the intrinsic scatter of the correlations used in the average procedure, as it is this term that typically dominates the error budget. At the present time, we should give the correlations with the larger $\sigma_{\rm int}$ values (e.g. the *L*–*V* one), but this would lower the number of objects in the sample and increase the error because of averaging over a lower number of μ estimates. Larger GRB samples with measured redshift and observational parameters are then needed to address the issue of the impact of calibration methods on a safer basis.

5.2 Impact of the averaging procedure

As stated above, averaging the μ values from different correlations helps to reduce the total uncertainties and partially removes the systematics connected to each single scaling relation. However, this does not come without a price. Indeed, such a strategy implicitly assumes that all the scaling relations are physical and not the artefact of a selection effect that is not well controlled. This danger is actually hard to avoid as no clearly defined and well-accepted theoretical model is presently available to describe the physics of GRBs and to predict scaling relations in agreement with the empirically motivated ones.

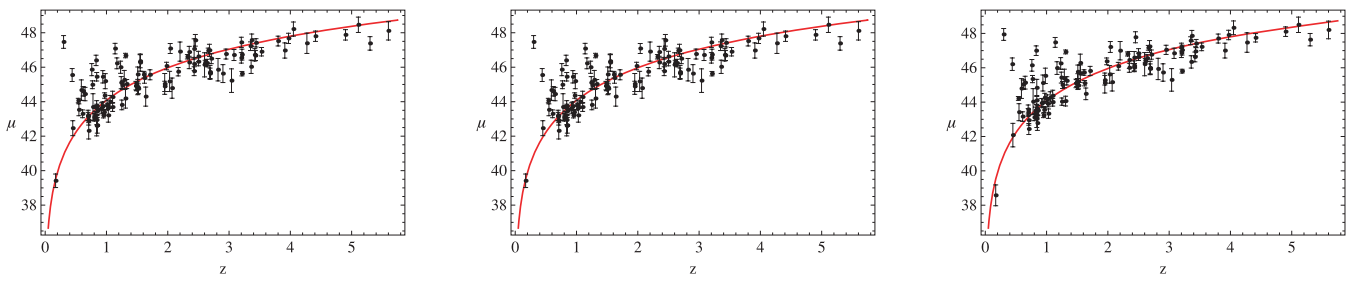

Figure 1. GRB HDs averaging over the six 2D correlations and excluding outliers (see text for the definition of outliers). The three panels refer to the HDs derived using the calibration based on the fiducial ΛCDM model (left), the cosmographic parameters (centre) and the local regression (right).

Table 4. Deviations from the fiducial ΛCDM distance modulus estimates for the different GRB 2D correlations used, adopting the calibration method based on the fiducial luminosity distances (i.e. the *F* sample). We report the number of GRBs and the mean, median and rms values.

ID	$\mathcal{N}$	$\langle\Delta\mu\rangle$	$(\Delta\mu)_{\rm med}$	$(\Delta\mu)_{\rm rms}$
L–$E_{\rm peak}$	115	−0.20	0.01	1.32
L–$\tau_{\rm lag}$	60	0.03	0.09	0.61
L–$\tau_{\rm RT}$	79	−0.12	0.07	0.94
L–V	115	−0.50	0.05	1.86
E_γ–$E_{\rm peak}$	30	0.04	0.28	0.97
$E_{\rm iso}$–$E_{\rm peak}$	100	−0.01	0.05	1.01

As a first check, we compare the $\Delta\mu$ values obtained by estimating μ using each single correlation. For the *F* sample, we obtain the results summarized in Table 4 where we also give the number of GRBs used. The conclusions are unaltered for the *C* and *LR* samples so we do not discuss them.

While the median values of $\Delta\mu$ are roughly comparable, both $\langle\Delta\mu\rangle$ and $(\Delta\mu)_{\rm rms}$ are definitely larger for the L–$E_{\rm peak}$ and L–V correlations. It is worth noting that these are also the only two correlations where all the GRBs can be used to infer the HD. So, we could ascribe the larger $(\Delta\mu)_{\rm rms}$ to the inclusion of a higher number of outliers. However, this same effect can be a statistical artefact because of the use of a smaller GRB sample. It is actually hard to understand whether a selection effect is at work here. Indeed, the inclusion of a GRB in a sample used for a given correlation depends mainly on observational requirements (e.g. the GRB afterglow should last long enough to measure the rise time). So, we could argue that this has nothing to do with its departure from a theoretical quantity, such as the fiducial distance modulus. However, should selection effects induce a fake correlation, we can imagine that the deviations from the fiducial curve would be randomly distributed, leading to small $\langle\Delta\mu\rangle$.

Before asking which relation is physical, we can quantify the impact of an incorrect assumption by evaluating again the distance moduli excluding the L–V and L–$E_{\rm peak}$ correlations. As these are the ones with the greatest rms $\Delta\mu$ and the largest intrinsic scatter (see Table 1), we expect them to have the greatest impact on the departure from the fiducial ΛCDM theoretically predicted HD. We find

$$\langle\Delta\mu\rangle = -0.11, \qquad (\Delta\mu)_{\rm med} = 0.04, \qquad (\Delta\mu)_{\rm rms} = 1.05,$$

for 106 GRBs, a number that is smaller than before because some GRBs with μ determined from the L–$E_{\rm peak}$ and/or L–V correlations only now drop out of the final sample. Compared with the case with all correlations included, the mean, median and rms $\Delta\mu$ are indeed smaller. However, as we average now on a lower number of correlations, the uncertainty on μ for each GRB is now larger, so that the $\Delta\mu$ values with and without these two correlations are consistent within the 1σ confidence ranges.

We must therefore conclude that, given the available GRB data set, the decision of whether or not to include a given correlation in the averaging procedure should be a compromise between the need to avoid an uncertain systematic bias and the desire to ameliorate both statistics and precision.

5.3 Satellite dependence

The XS09 GRB sample is compiled by collecting the data available in the literature, so the final catalogue is not homogeneous at all. In particular, the satellite used to obtain both the spectral and afterglow data changes from one case to another. In order to investigate whether this could have any impact on the HD, we consider again the deviations from the fiducial ΛCDM model using only the 80 GRBs detected with the *Swift* satellite (excluding outliers). We obtain

$$\langle\Delta\mu\rangle = -0.29, \qquad (\Delta\mu)_{\rm med} = 0.03, \qquad (\Delta\mu)_{\rm rms} = 1.33,$$

$$\langle\Delta\mu\rangle = -0.24, \qquad (\Delta\mu)_{\rm med} = 0.11, \qquad (\Delta\mu)_{\rm rms} = 1.32,$$

$$\langle\Delta\mu\rangle = -0.40, \qquad (\Delta\mu)_{\rm med} = 0.05, \qquad (\Delta\mu)_{\rm rms} = 1.40,$$

including all correlations and using the *F*, *C* and *LR* samples, respectively. We find

$$\langle\Delta\mu\rangle = -0.25, \qquad (\Delta\mu)_{\rm med} = -0.05, \qquad (\Delta\mu)_{\rm rms} = 1.18,$$

$$\langle\Delta\mu\rangle = -0.18, \qquad (\Delta\mu)_{\rm med} = 0.06, \qquad (\Delta\mu)_{\rm rms} = 1.18,$$

$$\langle\Delta\mu\rangle = -0.33, \qquad (\Delta\mu)_{\rm med} = -0.05, \qquad (\Delta\mu)_{\rm rms} = 1.24,$$

when excluding the L–$E_{\rm peak}$ and L–V correlations and the same samples. Surprisingly, we find larger $\Delta\mu$ values independent of the calibration procedure adopted and of the use of all or only four out of the six scaling laws. Actually, this is most likely a consequence of the different redshift range probed. Indeed, $\Delta\mu$ positively correlates with z so that a sample with a larger median redshift will have a larger $\langle\Delta\mu\rangle$. This is indeed the case here, as the pre-*Swift* data are limited to a smaller redshift range, mainly because of instrumental effects. We therefore agree with the results of XS09. They have argued against a systematic difference among pre- and post-*Swift* GRB data sets.

6 CONCLUSIONS

GRBs have recently attracted much attention as promising candidates for expanding the HD up to very high z, deep into the matter-dominated era. Thus, they would complement SNe Ia, which are, in contrast, excellent probes of the dark energy epoch. However, much work still needs to be done in order to be sure that GRBs can indeed deliver this promise.

As the Phillips law is the basic tool to standardize SNe Ia, the hunt for a similar relation to be used for GRBs has led to different empirically motivated 2D scaling relations. However, the lack of a local GRB sample has led to the so-called circularity problem (i.e. the need to know the cosmological model to infer the luminosity distance to each GRB, contrasted with the desire to constrain that same cosmological model). In an attempt to overcome this problem, here we have considered the impact on the scaling relations and GRB HD of three different methods for estimating the luminosity distance. First, we rely on a fiducial ΛCDM model fitted to the SNe Ia data. Then, we take a step further towards a model-independent calibration using the cosmographic expansion to the fifth-order in z, thus only assuming that the Robertson–Walker metric describes the Universe background. Finally, we use local regression on SNe Ia to interpolate the luminosity distance to a given z with no assumption at all on the cosmological model. We find that these three conceptually different methods for estimating the

luminosity distance, and hence calibrating the GRB scaling relations, lead to consistent results. Indeed, the slope, zero-point and intrinsic scatter of the 2D correlations are in good agreement within the 68 per cent confidence range. As a consequence, the HD averaging over the six correlations considered is not affected by the choice of the calibration method, with the distance moduli to each GRB being in agreement within the errors. Such a preliminary conclusion might suggest that the calibration problem could actually be a false problem, as the use of a fiducial model to estimate the luminosity distance to the $z \leq 1.4$ GRBs finally leads to the same HD of a fully model-independent method, such as the local regression. Actually, some important caveats have to be taken into account in order not to overrate this result. First, we have chosen as a fiducial model the concordance ΛCDM model, which is known to fit the SNe Ia data very well. As such, the predicted luminosity distance closely follows that inferred from SNe Ia, which can be estimated using local regression. As such, these two apparently different luminosity distance methods actually give the same luminosity distance values. Thus, the agreement of the constraints on the GRB parameters is not surprising. If we had used as the fiducial model a different dark energy scenario, the results could have been different. Moreover, although not statistically meaningful, a weak dependence of the slope of the GRB scaling relations on the calibration method is indeed present, with the local regression leading to shallower relations. A larger GRB sample is therefore needed to check whether these trends are only a statistically meaningless fluctuation or evidence of the key role of the calibration method adopted.

Once the calibration procedure has been adopted, we still have to check whether a redshift evolution of the GRB scaling relations is present or not. Indeed, should the scaling relation coefficients be a function of z, neglecting such a dependence would bias both the calibration and the HD, thus introducing a systematic error when using the derived HD to constrain the cosmological parameters. We have therefore explored two different parameterizations, assuming that the zero-point only changes with z or that both the slope and the zero-point can be approximated as linear functions of the redshift. Although there is evidence in favour of a significant evolution of the zero-point with the redshift, it is nevertheless worth stressing that adding one or two more parameters to the fit of the scaling relations does not improve the quality of the fit (the reduced χ^2 being the same or larger) and it does not reduce the intrinsic scatter. Occam's razor therefore makes us argue that such an evolution is not statistically motivated, and neglecting it is actually a conservative and better motivated choice. It is, however, worth noting that such a conclusion relies heavily on the quality of the data. Indeed, the value of χ^2 also depends on the size of the uncertainties. For instance, artificially reducing by hand the errors, leaving the central values unchanged, increases the statistical significance of the redshift evolution, making this choice the most conservative. However, we should reconsider this issue by preliminarily investigating whether a selection effect is present. Indeed, we have implicitly assumed that the probability to measure the quantities entering the fitted correlation is the same whatever the GRB redshift is. Should this not be the case, we have to include a prior in the likelihood function to model this selection effect and to check whether the results are affected or not by the prior itself. However, such an analysis can only be made on a case-by-case basis and it needs a preliminary theoretical modelling of the correlation of interest to simulate the full detection process.

Assuming that no evolution is present, we have finally checked that the derived HDs are not affected by systematics related to the choice of the calibration method, the averaging procedure or the homogeneity of the sample. As such, the GRB HD can be safely used as a tool to constrain cosmological parameters. Although these results are very encouraging, we warn the reader that they are still preliminary. Indeed, what we have actually shown is that the systematics induced by the different effects we have considered are smaller than the statistical errors resulting from the measurement uncertainties of the GRB observable quantities and the intrinsic scatter of the 2D scaling relations used. It is not possible to forecast whether the conclusions still hold if these errors are reduced. To this end, increasing the number of GRBs and improving the precision might not be the right strategy. Indeed, the error budget on the distance modulus is typically dominated by the intrinsic scatter, so we should perhaps rely on GRB scaling relations that are as tight as possible. From this point of view, for instance, we should give away the L–$E_{\rm peak}$ and L–V correlations. However, this comes at the price of reducing the number of usable GRBs and increasing the error (as we now average on a lower number of μ estimates). Again, this leads to the need for larger GRB samples to select the tightest correlations without degrading the precision on the distance modulus determination.

As a final remark, an analogy between SNe Ia and GRBs as cosmological tools can be considered. As soon as the Phillips law was established, SNe Ia started to be used to probe the HD up to $z \sim 1.5$, notwithstanding possible problems with the evolution of the standardization method adopted and the universality of its basic assumptions. Nowadays, SNe Ia samples have so many objects that it is possible not only to use them as cosmological tools, but also to carefully explore systematics and their impact on the HD. The present-day situation for GRBs is similar to many Phillips law-like relations proposed to standardize them; most attention is dedicated more to their cosmological use than to the systematics. As for SNe Ia, we must therefore only wait until, as time goes by and new instruments bring us larger and higher-quality samples, the issue of GRB systematics can be more efficiently examined. This might show that these powerful explosions do indeed promise to fill the gap between the dark energy era probed by SNe Ia and the early Universe tested by CMBR.

ACKNOWLEDGMENT

VFC is supported by the Italian Space Agency (ASI).

REFERENCES

Aldering G. et al., 2004, preprint (astro-ph/0405232); see also http://snap.lbl.gov
Amanullah R. et al., 2010, ApJ, 716, 712
Amati L., Guidorzi C., Frontera F., Della Valle M., Finelli F., Landi R., Montanari E., 2008, MNRAS, 391, 577
Amati L., Frontera F., Guidorzi C., 2009, A&A, 508, 173
Band D. et al., 1993, ApJ, 413, 281
Bouhmadi-López M., Capozziello S. Cardone V. F., 2010, Phys. Rev. D, 82, 103526
Brown M. L. et al., 2009, ApJ, 705, 978
Capozziello S., Francaviglia M., 2008, Gen. Relat. Gravit., 40, 357
Capozziello S., Cardone V. F., Salzano V., 2008, Phys. Rev. D, 78, 063504
Cardone V. F., Capozziello S., Dainotti M. G., 2009, MNRAS, 400, 775 (CCD09)
Carroll S. M., Press W. H., Turner E. L., 1992, ARA&A, 30, 499
Chevallier M., Polarski D., 2001, Int. J. Mod. Phys. D, 10, 213
Cleveland W. S., 1979, J. Amer. Stat. Ass., 74, 829

Cleveland W. S., Devlin S. J., 1988, J. Amer. Stat. Ass., 83, 596
Copeland E. J., Sami M., Tsujikawa S., 2006, Int. J. Mod. Phys. D, 15, 1753
D'Agostini G., 2005, preprint (arXiv:physics/0511182)
Dainotti M. G., Cardone V. F., Capozziello S., 2008, MNRAS, 391, L79
Dainotti M. G., Willingale R., Cardone V. F., Capozziello S., Ostrowski M., 2010, ApJ, 722, L215
Dainotti M. G., Cardone V. F., Capozziello S., Ostrowski M., Willingale R., 2011, ApJ, 730, 135
de Bernardis P. et al., 2000, Nat, 404, 955
De Felice A., Tsujikawa S., 2010, Living Reviews in Relativity, 13, 3
Diaferio A., Ostorero L., Cardone V. F., 2011, preprint (arXiv:1103.5501)
Dodelson S. et al., 2002, ApJ, 572, 140
Eisenstein D. J. et al., 2005, ApJ, 633, 560
Fenimore E. E., Ramirez-Ruiz E., 2000, ApJ, 539, 712
Firmani C., Ghisellini G., Avila Reese V., Ghirlanda G., 2006, MNRAS, 370, 185
Gelman A., Rubin D. B., 1992, Statistical Sci., 7, 457
Ghirlanda G., Ghisellini G., Lazzati D., 2004, ApJ, 616, 331
Ghirlanda G., Ghisellini G., Firmani C., 2006, New J. Phys., 8, 123
Hawkins E. et al., 2003, MNRAS, 346, 78
Hicken M., Wood-Vasey W. M., Blondin S., Challis P., Jha S., Kelly P. L., Rest A., Kirshner R. P., 2009, ApJ, 700, 1097
Izzo L., Capozziello S., Covone G., Capaccioli M., 2009, A&A, 508, 63
Kessler R. et al., 2009, ApJS, 185, 32
Kodama Y., Yonetoku D., Murakami T., Tanabe S., Tsutsui R., Nakamura T., 2008, MNRAS, 391, L1
Komatsu E. et al., 2011, ApJS, 192, 18
Kowalski M. et al., 2008, ApJ, 686, 749
Liang E., Zhang B., 2005, ApJ, 633, 611
Liang N., Xiao W. K., Liu Y., Zhang S. N., 2008, ApJ, 385, 654
Liang N., Wu P., Zhang S. N., 2010, Phys. Rev. D, 81, 083518
Linder E. V., 2003, Phys. Rev. Lett., 90, 091301
Loader C., 1999, Local Regression and Likelihood. Springer, Berlin
Nojiri S., Odintsov S. D., 2008, in Problems of Modern Theoretical Physics, A Volume in Honour of Professor I. L. Buchbinder on the occasion of his 60th birthday. TSPU Publishing, Tomsk, p. 266 (arXiv:0807.0685)
Norris J. P., Marani G. F., Bonnell J. T., 2000, ApJ, 534, 248
Peebles P. J. E., Ratra B., 2003, Rev. Mod. Phys., 75, 559
Percival W. J. et al., 2002, MNRAS, 337, 1068
Percival W. J. et al., 2007, ApJ, 657, 645
Percival W. J. et al., 2010, MNRAS, 401, 2148
Qi S., Lu T., 2010, ApJ, 717, 1274
Reichart D. E., Lamb D. Q., Fenimore E. E., Ramirez-Ruiz E., Cline T. L., Hurley K., 2001, ApJ, 552, 57
Riess A. G. et al., 2009, ApJ, 699, 539
Sahni V., Starobinsky A. A., 2000, Int. J. Mod. Phys. D, 9, 373
Salvaterra R. et al., 2009, Nat, 461, 1258
Schaefer B. E., 2003, ApJ, 583, L67
Schaefer B. E., 2007, ApJ, 660, 16 (S07)
Sotiriou T., Faraoni V., 2010, Rev. Mod. Phys., 82, 451
Szalay A. S. et al., 2003, ApJ, 591, 1
Tegmark M. et al., 2006, Phys. Rev. D, 74, 123507
Visser M., 2004, Class. Quant. Grav., 21, 2603
Vitagliano V., Xia J. Q., Liberati S., Viel M., 2010, JCAP, 1003, 005
Wei H., Zhang S. N., 2009, Eur. Phys. J. C, 63, 139
Weinberg S., 1972, Gravitation and Cosmology. Wiley, New York
Xiao L., Schaefer B. E., 2009, ApJ, 707, 387 (XS09)
Xu L., Wang Y., 2010, preprint (arXiv:1009.0963)
Yonetoku D., Muramaki T., Nakamura T., Yamazaki R., Inoue A. K., Ioka K., 2004, ApJ, 609, 935

APPENDIX A:

For completeness, here we report the constraints on the calibration parameters for the two different redshift evolution parameterizations

Table A1. Constraints on the calibration parameters (a, b, α, $\sigma_{\rm int}$) for the 2D correlations considered in the text and fitted to the *F*, *C* and *LR* samples (first, second and third rows of each fit). The columns are as follows: (1) correlation ID; (2) reduced χ^2; (3) best-fitting parameters; (4)–(7) median values and 68 per cent confidence ranges for the fit parameters. The number of GRBs used is the same as in Table 1.

ID	χ^2/d.o.f.	$(a, b, \alpha, \sigma_{\rm int})_{\rm bf}$	a	b	α	$\sigma_{\rm int}$
L–$E_{\rm peak}$	1.08	(0.89, 50.77, 0.67, 0.41)	$0.82^{+0.20}_{-0.19}$	$50.75^{+0.59}_{-0.65}$	$0.68^{+0.18}_{-0.30}$	$0.44^{+0.06}_{-0.06}$
L–$E_{\rm peak}$	1.13	(0.90, 50.84, 0.61, 0.40)	$0.83^{+0.22}_{-0.19}$	$50.84^{+0.55}_{-0.60}$	$0.62^{+0.32}_{-0.29}$	$0.43^{+0.07}_{-0.05}$
L–$E_{\rm peak}$	1.17	(0.75, 50.88, 0.65, 0.38)	$0.66^{+0.19}_{-0.17}$	$50.78^{+0.63}_{-0.65}$	$0.72^{+0.34}_{-0.34}$	$0.41^{+0.05}_{-0.06}$
L–$\tau_{\rm lag}$	1.10	(−0.58, 50.38, 0.88, 0.39)	$-0.57^{+0.12}_{-0.14}$	$50.39^{+0.66}_{-0.58}$	$0.87^{+0.30}_{-0.33}$	$0.41^{+0.07}_{-0.06}$
L–$\tau_{\rm lag}$	1.19	(−0.58, 50.39, 0.85, 0.38)	$-0.54^{+0.13}_{-0.13}$	$50.31^{+0.57}_{-0.56}$	$0.89^{+0.29}_{-0.28}$	$0.41^{+0.07}_{-0.06}$
L–$\tau_{\rm lag}$	1.24	(−0.55, 50.45, 0.88, 0.31)	$-0.52^{+0.11}_{-0.12}$	$50.38^{+0.53}_{-0.50}$	$0.91^{+0.25}_{-0.27}$	$0.33^{+0.07}_{-0.05}$
L–$\tau_{\rm RT}$	1.16	(−0.79, 51.22, 0.65, 0.44)	$-0.64^{+0.21}_{-0.25}$	$50.97^{+0.70}_{-0.75}$	$0.76^{+0.36}_{-0.33}$	$0.47^{+0.07}_{-0.06}$
L–$\tau_{\rm RT}$	1.13	(−0.72, 51.08, 0.69, 0.45)	$-0.63^{+0.18}_{-0.22}$	$50.97^{+0.64}_{-0.66}$	$0.73^{+0.34}_{-0.30}$	$0.47^{+0.08}_{-0.06}$
L–$\tau_{\rm RT}$	1.20	(−0.76, 51.32, 0.64, 0.36)	$-0.66^{+0.20}_{-0.24}$	$51.20^{+0.71}_{-0.80}$	$0.68^{+0.38}_{-0.34}$	$0.40^{+0.07}_{-0.06}$
L–V	1.23	(−0.10, 50.27, 1.07, 0.54)	$-0.05^{+0.26}_{-0.37}$	$50.29^{+0.91}_{-0.96}$	$1.04^{+0.52}_{-0.50}$	$0.57^{+0.11}_{-0.08}$
L–V	1.23	(−0.14, 50.31, 1.05, 0.54)	$-0.09^{+0.16}_{-0.37}$	$50.26^{+0.82}_{-0.82}$	$1.07^{+0.47}_{-0.46}$	$0.57^{+0.10}_{-0.08}$
L–V	1.36	(−0.10, 50.32, 1.10, 0.42)	$-0.10^{+0.12}_{-0.30}$	$50.38^{+0.70}_{-0.76}$	$1.07^{+0.41}_{-0.42}$	$0.46^{+0.09}_{-0.07}$
E_γ–$E_{\rm peak}$	1.37	(1.57, 50.64, 0.00, 0.14)	$1.48^{+0.23}_{-0.26}$	$50.42^{+0.51}_{-0.57}$	$0.13^{+0.31}_{-0.28}$	$0.20^{+0.07}_{-0.06}$
E_γ–$E_{\rm peak}$	1.38	(1.60, 50.66, −0.01, 0.14)	$1.44^{+0.24}_{-0.29}$	$50.34^{+0.48}_{-0.68}$	$0.16^{+0.37}_{-0.25}$	$0.21^{+0.08}_{-0.07}$
E_γ–$E_{\rm peak}$	1.35	(1.58, 50.74, −0.03, 0.12)	$1.47^{+0.24}_{-0.25}$	$50.46^{+0.52}_{-0.61}$	$0.12^{+0.33}_{-0.29}$	$0.19^{+0.09}_{-0.08}$
$E_{\rm iso}$–$E_{\rm peak}$	0.81	(1.39, 51.58, 0.58, 0.48)	$1.29^{+0.28}_{-0.28}$	$51.57^{+0.84}_{-0.81}$	$0.58^{+0.44}_{-0.45}$	$0.50^{+0.10}_{-0.08}$
$E_{\rm iso}$–$E_{\rm peak}$	0.81	(1.40, 51.70, 0.50, 0.48)	$1.28^{+0.28}_{-0.29}$	$51.43^{+0.75}_{-0.81}$	$0.64^{+0.43}_{-0.40}$	$0.50^{+0.10}_{-0.08}$
$E_{\rm iso}$–$E_{\rm peak}$	0.80	(1.41, 51.98, 0.37, 0.47)	$1.32^{+0.28}_{-0.30}$	$51.89^{+0.75}_{-0.86}$	$0.42^{+0.46}_{-0.39}$	$0.50^{+0.10}_{-0.08}$

Table A2. Constraints on the calibration parameters (a_0, $\log a_1$, b_0, $\log b_1$, $\sigma_{\rm int}$) for the 2D correlations considered in the text and fitted to the *F*, *C* and *LR* samples (first, second and third rows of each fit). The columns are as follows: (1) correlation ID; (2) reduced χ^2; (3) best-fitting parameters; (4)–(8) median values and 68 per cent confidence ranges for the fit parameters. The number of GRBs used is the same as in Table 1.

ID	χ^2/d.o.f.	$(a_0, \log a_1, b_0, \log b_1, \sigma_{\rm int})_{\rm bf}$	a_0	$\log a_1$	b_0	$\log b_1$	$\sigma_{\rm int}$
L–$E_{\rm peak}$	1.12	(0.89, −2.69, 51.49, −0.21, 0.41)	$0.89^{+0.22}_{-0.25}$	$-3.05^{+2.13}_{-3.63}$	$51.87^{+0.19}_{-0.46}$	$-0.78^{+0.64}_{-3.06}$	$0.44^{+0.03}_{-0.05}$
L–$E_{\rm peak}$	1.13	(0.62, −0.57, 51.44, −0.20, 0.41)	$0.84^{+0.23}_{-0.27}$	$-2.83^{+2.67}_{-4.19}$	$51.83^{+0.20}_{-0.44}$	$-0.71^{+0.55}_{-3.02}$	$0.44^{+0.06}_{-0.06}$
L–$E_{\rm peak}$	1.18	(0.73, −2.71, 51.50, −0.16, 0.38)	$0.75^{+0.21}_{-0.23}$	$-2.76^{+1.75}_{-3.39}$	$52.00^{+0.16}_{-0.50}$	$-1.05^{+0.89}_{-3.76}$	$0.41^{+0.06}_{-0.05}$
L–$\tau_{\rm lag}$	1.13	(−0.60, −4.43, 51.31, −0.07, 0.40)	$-0.64^{+0.16}_{-0.19}$	$-2.78^{+1.61}_{-2.85}$	$51.61^{+0.49}_{-0.45}$	$-0.28^{+0.27}_{-2.83}$	$0.43^{+0.08}_{-0.06}$
L–$\tau_{\rm lag}$	1.21	(−0.61, −2.61, 51.25, −0.07, 0.39)	$-0.59^{+0.13}_{-0.14}$	$-3.13^{+1.72}_{-3.50}$	$51.43^{+0.50}_{-0.37}$	$-0.17^{+0.18}_{-0.82}$	$0.42^{+0.08}_{-0.06}$
L–$\tau_{\rm lag}$	1.30	(−0.74, −0.60, 51.27, −0.02, 0.31)	$-0.58^{+0.13}_{-0.14}$	$-2.98^{+1.84}_{-4.55}$	$51.47^{+0.45}_{-0.32}$	$-0.13^{+0.11}_{-0.42}$	$0.34^{+0.08}_{-0.06}$
L–$\tau_{\rm RT}$	1.17	(−1.56, −0.08, 52.38, −0.70, 0.44)	$-0.95^{+0.33}_{-0.46}$	$-1.81^{+1.59}_{-3.90}$	$52.42^{+0.19}_{-0.53}$	$-1.81^{+1.60}_{-3.91}$	$0.47^{+0.07}_{-0.06}$
L–$\tau_{\rm RT}$	1.22	(−1.59, −0.07, 52.29, −0.63, 0.44)	$-0.82^{+0.27}_{-0.35}$	$-2.36^{+1.86}_{-3.33}$	$52.28^{+0.23}_{-0.60}$	$-0.92^{+0.79}_{-3.36}$	$0.47^{+0.08}_{-0.06}$
L–$\tau_{\rm RT}$	1.27	(−1.83, 0.07, 52.60, −2.77, 0.33)	$-1.09^{+0.17}_{-0.60}$	$-0.89^{+0.89}_{-3.90}$	$52.54^{+0.16}_{-0.35}$	$-2.43^{+2.04}_{-4.07}$	$0.39^{+0.07}_{-0.06}$
L–V	1.36	(−0.15, −2.16, 51.40, 0.03, 0.52)	$-0.10^{+0.41}_{-0.44}$	$-1.79^{+1.49}_{-4.81}$	$51.85^{+0.39}_{-0.53}$	$-0.77^{+0.76}_{-2.86}$	$0.58^{+0.10}_{-0.08}$
L–V	1.24	(−0.11, −2.68, 51.32, 0.02, 0.56)	$-0.21^{+0.44}_{-0.47}$	$-2.15^{+1.49}_{-3.78}$	$51.85^{+0.39}_{-0.53}$	$-0.77^{+0.76}_{-2.86}$	$0.58^{+0.10}_{-0.08}$
L–V	1.40	(−0.13, −3.13, 51.40, 0.06, 0.43)	$-0.02^{+0.40}_{-0.44}$	$-1.94^{+1.56}_{-2.39}$	$51.86^{+0.41}_{-0.46}$	$-0.57^{+0.59}_{-3.83}$	$0.49^{+0.10}_{-0.08}$
E_γ–$E_{\rm peak}$	1.70	(0.79, 0.04, 50.37, −0.56, 0.10)	$1.40^{+0.23}_{-0.47}$	$-1.70^{+1.63}_{-2.67}$	$50.61^{+0.08}_{-0.15}$	$-2.86^{+1.91}_{-3.84}$	$0.17^{+0.08}_{-0.06}$
E_γ–$E_{\rm peak}$	1.49	(0.98, −0.05, 50.46, −0.92, 0.12)	$1.43^{+0.22}_{-0.49}$	$-2.42^{+2.36}_{-4.22}$	$50.59^{+0.08}_{-0.12}$	$-2.98^{+2.91}_{-3.35}$	$0.17^{+0.08}_{-0.06}$
E_γ–$E_{\rm peak}$	1.70	(0.74, 0.09, 50.40, −0.57, 0.06)	$1.47^{+0.19}_{-0.37}$	$-2.70^{+2.41}_{-4.51}$	$50.64^{+0.08}_{-0.12}$	$-2.90^{+1.69}_{-4.00}$	$0.16^{+0.09}_{-0.07}$
$E_{\rm iso}$–$E_{\rm peak}$	0.79	(0.94, −0.23, 52.00, −0.15, 0.49)	$1.27^{+0.33}_{-0.50}$	$-1.78^{+1.61}_{-2.54}$	$52.56^{+0.16}_{-0.34}$	$-1.73^{+1.42}_{-2.41}$	$0.50^{+0.10}_{-0.08}$
$E_{\rm iso}$–$E_{\rm peak}$	0.91	(0.69, −0.07, 51.98, −0.12, 0.44)	$1.20^{+0.39}_{-0.92}$	$-1.36^{+1.47}_{-3.41}$	$52.53^{+0.16}_{-0.43}$	$-1.93^{+1.67}_{-3.31}$	$0.49^{+0.08}_{-0.07}$
$E_{\rm iso}$–$E_{\rm peak}$	0.86	(0.66, −0.05, 52.21, −0.28, 0.45)	$1.24^{+0.34}_{-0.72}$	$-1.85^{+1.85}_{-2.98}$	$52.57^{+0.17}_{-0.39}$	$-1.84^{+1.56}_{-2.80}$	$0.49^{+0.10}_{-0.08}$

and the three luminosity distance estimate methods. Although the best-fitting values might be different from one case to another, the confidence ranges for the parameters always overlap quite well, so that the difference is not statistically meaningful. The main conclusions in Section 4 also qualitatively apply, changing the calibration method so that we do not repeat the analysis of the results.

This paper has been typeset from a TEX/LATEX file prepared by the author.